Materials Letters 290 (2021) 129451

Contents lists available at ScienceDirect

Materials Letters

journal homepage: www.elsevier.com/locate/mlblue

Forming the locally-gradient Ni@$NiTe_2$ domains from initial Ni inclusions embedded into thermoelectric Bi_2Te_3 matrix

Maxim Yaprintsev [a], Alexei Vasil'ev [b], Oleg Ivanov [b,*], Marina Zhezhu [a], Ekaterina Yaprintseva [b], Vseslav Novikov [a]

[a] Belgorod State University, Belgorod 394015, Russian Federation
[b] Belgorod State Technological University named after V.G. Shukhov, Belgorod 308012, Russian Federation

ARTICLE INFO

Article history:
Received 26 November 2020
Received in revised form 28 January 2021
Accepted 29 January 2021
Available online 8 February 2021

Keywords:
Composite materials
Interfaces
"Core"–"shell" inclusions
Locally-gradient domains
Thermoelectric properties

ABSTRACT

Mixtures of thermoelectric Bi_2Te_3 powder and ferromagnetic Ni powder were spark-plasma-sintered to prepare bulk composites with different Ni content (0.00, 0.50, 0.85, 1.25 and 1.50 at.%). Hexagonal Bi_2Te_3, cubic Ni and trigonal $NiTe_2$ phases coexist in the composites. Bi_2Te_3 phase forms matrix of the composite, whereas Ni and $NiTe_2$ phases correspond to filler. The filler is formed by locally-gradient Ni@$NiTe_2$ ("core–shell") inclusions. Forming the "core–shell" inclusions is due to high-temperature diffusion redistribution of matrix and filler atoms during the composites sintering. The thermoelectric figure-of-merit of the composites with the locally-gradient inclusions is remarkably enhanced as compared to that of the Bi_2Te_3 matrix.

1. Introduction

Constructing various composites is effective way to develop functional or structural materials with characteristics, which can be remarkably enhanced as compared to relevant characteristics of matrix and filler materials, applied to construct the composite [1]. Besides combining properties, which are inherent to the matrix and filler materials, new interesting and helpful properties due to matrix/filler interfaces can be observed in the composites. Usually, the composite consists of the matrix with the filler inclusions having specific size and shape, which are randomly distributed inside the matrix. During fabrication of the composite, any chemical interaction between the matrix and filler materials should be minimized to retain the sharp expressed matrix/filler interfaces. In this case, all the filler material is spatially concentrated inside the inclusion, i.e. no diffusion redistribution of matrix and filler atoms occurs. If diffusion redistribution can be initiated, the filler material will start diffusing into the matrix and the matrix material will start diffusing into the filler. As result, a gradient distribution of concentration of elements being diffused is formed within some spatial domain. This domain can be called as a locally-gradient domain (LGD). Size and properties of the LGD will be dependent on parameters that affect diffusion processes during fabrication of the composite. Among dominant parameters, the matrix and filler materials properties, temperature and holding time of the fabrication can be listed. Varying the parameters, the properties of the composite can be additionally tuned via forming system of the LGDs with desired size, structure, phase and elemental composition. Aim of this work is to examine forming the LGDs during fabrication of bulk composite consisting of the Bi_2Te_3 matrix with the Ni inclusions. The matrix material is applied to prepare *n*-$Bi_2Te_{3-x}Se_x$ and *p*-$Bi_{2-x}Sb_xTe_3$ alloys for low-temperature thermoelectric applications [2], whereas the filler material is ferromagnet with the Curie temperature at 628 K [3]. The thermoelectric properties of the composites were also tested.

2. Material and methods

To prepare the composites with different Ni content, x (x = 0.00, 0.50, 0.85, 1.25 and 1.50 at.%), individual Bi_2Te_3 and Ni powders were preliminary synthesized. To synthesize the Bi_2Te_3 powder, Bi_2O_3, SeO_2, TeO_2 precursors were firstly dissolved in ethylene glycol with some addition of alkaline agent (KOH) to control pH-value. Obtained solution was transferred to round-bottom flask and heated to boiling point. After evaporation of water impurity, flask with solution sealed with reflux and maintained at 458 K for 4 h. Resulted dark suspension was cooled to room temperature. The

* Corresponding author.
E-mail address: Ivanov.Oleg@bsu.edu.ru (O. Ivanov).

https://doi.org/10.1016/j.matlet.2021.129451
0167-577X/

powder was purified by filtration and washing for 3 times with ethanol and acetone, and dried in argon atmosphere at 523 K for 2 h. To synthesize the Ni powder, 5 g $Ni(NO_3)_2$ $6H_2O$ was firstly dissolved in 400 ml ethylene glycol. Subsequently, 10 g KOH was added into solution. Mixture was heated to 353 K under vigorously stirring to homogeneity. Then, resulted sol was cooled to room temperature. Hydrazine hydrate was slowly added follow. Reaction mixture was heated to 373 K and maintained to 1 h to complete reduction process from Ni^{2+} to Ni^0. Obtained powder was collected by neodymium magnet and washed with ethanol and acetone to remove organic impurities. To prepare bulk composites, the Bi_2Te_3 and Ni powders were thoroughly mixed by planetary mill for 30 min. The mixed Bi_2Te_3 + Ni powders were spark-plasma-sintered (SPS) at pressure of 40 MPa and temperature of 573 K for 2 min.

X-ray diffraction (XRD) analysis of starting powders and bulk samples was carried out by Rigaku Ultima IV diffractometer with CuK_α – radiation. To examine morphology of starting powders, transmission electron microscopy (TEM) was applied by model JEM - 2100 microscope. Scanning electron microscopy (SEM, Nova NanoSEM 450 microscope) was applied to examine grain structure of bulk samples, distinguish different phases related to filler inclusions (by backscattered electron (BSE) method) and take profiles of elements, distributed along line crossing inclusions (by energy dispersive X-ray spectroscopy (EDS) method). The specific electrical resistivity and Seebeck coefficient were measured by using ZEM-3 system, whereas the total thermal conductivity was measured by TC-1200 system.

3. Results and discussion

The Bi_2Te_3 powder was single hexagonal $R\bar{3}m$ phase (Fig. 1(a)) with lattice a = 0.4354 nm and c = 30.035 nm parameters, and mainly consisted of hexagonal plate-shaped particles with sizes of 300–500 nm (Fig. 1(b)), whereas the Ni powder was single face-centered $Fm\bar{3}m$ cubic phase (Fig. 1(c)) with a = 0.3525 nm, and mainly consisted of agglomerated formations with sizes of 150–200 nm (Fig. 1(d)). Agglomerating many Ni particles is originated from a ferromagnetic interaction between the particles.

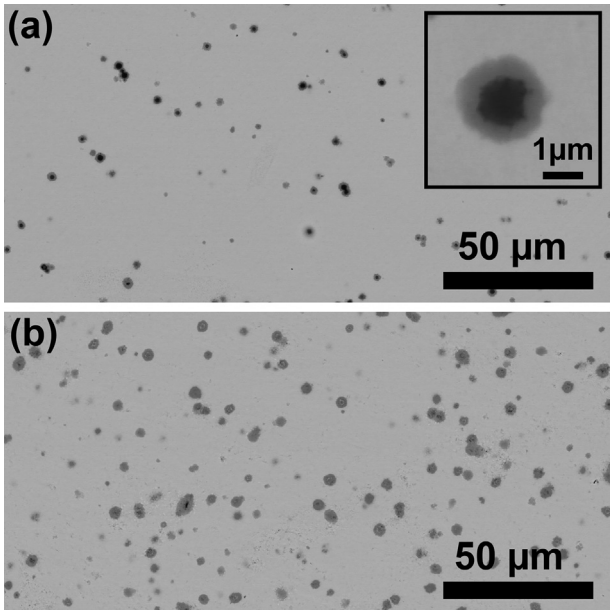

Fig. 1. XRD patterns and TEM images for the Bi_2Te_3 powder ((a) and (b)), and the Ni powder ((c) and (d)), and XRD pattern and SEM images for the composite with x = 1.25 at.% ((e), (f) and (g)).

Phase composition of bulk composites was found to be changed during SPS-process. Besides the initial Bi_2Te_3 and Ni phases, a new $NiTe_2$ phase is forming during the sintering (Fig. 1(e)). This phase has trigonal $P\bar{3}m1$ structure with lattice a = 0.3895 and c = 0.5470 nm parameters. Coexistence of three phases for the composite with x = 1.25 at.% is confirmed by analysis of XRD pattern (Fig. 1(e)). The pattern was taken from surface, oriented perpendicularly to SPS-pressuring direction. Additional peaks of the $NiTe_2$ phase, indicated by triangles, are observed. Due to small Ni content, Ni phase peaks are expressed weakly (inset to Fig. 1(e)). It is known that SPS-process results in texturing of Bi_2Te_3-based compounds, and texturing axis coincides with SPS-pressuring direction [4]. Texturing is observed in SEM images, recorded on fractured surfaces, which are oriented parallel and perpendicularly to SPS-pressing direction. These SEM images for the composite with x = 1.25 at.% are presented Fig. 1(f) and (g). Lamellar structure is formed at the parallel surface, and lamellar sheets with grains elongated along the surface, are oriented perpendicularly to SPS-pressuring direction. Disordered grain structure with grains having mainly irregular shape is observed at the perpendicular surface. Average lateral size and thickness of grains were estimated as ~ 500 and ~ 50 nm, respectively. BSE images for the composites with x = 0.5 and 1.25 at.% are shown in Fig. 2(a) and (b).

One can see that the composites are really constructed from matrix with embedded filler inclusions. A surface density of inclusions is higher for the composite with x = 1.25 at.%. Filler inclusions themselves were found to be composite (inset to Fig. 2(a)). During SPS-process, the inclusions form slightly distorted spherical "core" – "shell" structures. Average size of inclusions happened is larger for the composite with x = 1.25 at.%. A ratio between thickness of shell, l, and radius of core, r, is not constant and dependent on initial size of the Ni inclusions. Taking into account the l/d ratio, all the inclusions can be roughly separated by three main types. The inclusions of first type consist of big core, but thin shell, i.e. $d > l$. For second type, d and l are approximately equal to each other. In the inclusions of third type, the shell is dominated, i.e. $l > d$. To identify phase composition of the core and shell, EDS-line scanning carried out along line crossing the inclusions of three types. The inclusions and profiles of Bi, Te and Ni distributions are shown in Fig. 3.

For all the inclusions, Ni dominantly contains inside the core, whereas Ni and Te forming the $NiTe_2$ phase are dominated inside the shell. Far from the inclusion, Te and Bi are homogenously distributed, and Ni is missing. Therefore, the inclusions consisting of the Ni core covered with the $NiTe_2$ shell (Ni@$NiTe_2$ inclusions) are naturally formed in the composites. The Bi, Te and Ni distributions within the Ni@$NiTe_2$ inclusions are inhomogeneous, i.e. these inclusions are the LGDs. In contrast to functionally graded materials, gradient distributions are limited with size of the inclusion [5]. Forming the LGDs is originated from high-temperature diffusion redistribution of matrix and filler atoms, which occurs during SPS-process. The initial Ni inclusions should be considered as impurity Ni sources, which are randomly distributed inside the Bi_2Te_3 matrix. During SPS-process, the matrix and filler atoms start diffusing through matrix/filler interface. Due to diffusion redistri-

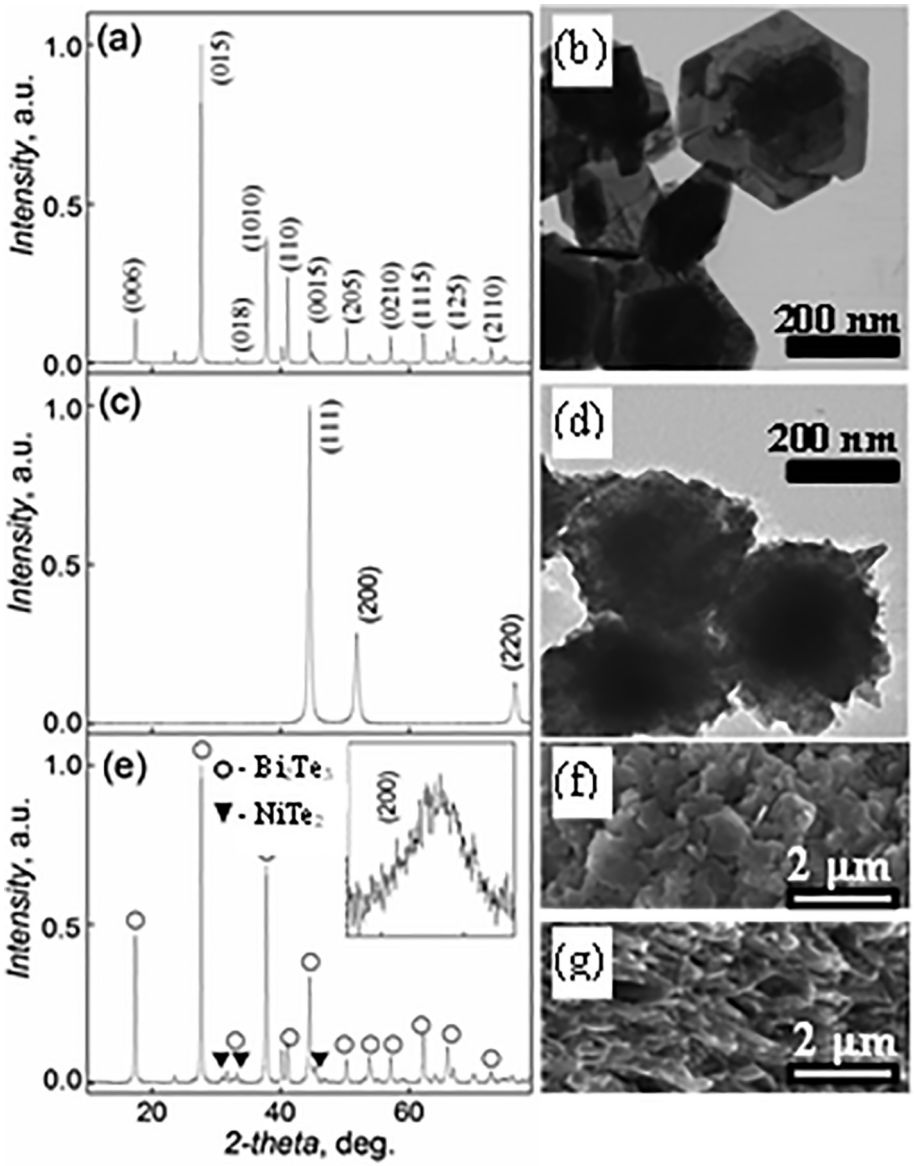

Fig. 2. BSE images for the composites with x = 0.5 and 1.25 at.%.

bution of atoms and chemical interaction between Bi_2Te_3 and Ni, the $NiTe_2$ phase is formed.

Currently, developing bulk thermoelectric composites is effective way to improve thermoelectric performance of thermoelectric materials [6]. Applying metallic inclusions, which possess ferro- or antiferromagnetic ordering, allows involving new thermoelectromagnetic effects. These effects can additionally improve the thermoelectric properties of the composite [7]. The thermoelectric properties of textured samples, measured parallel or perpendicularly to texturing axis, are known to be different and dependent on degree of preferential orientation of grains [4]. To estimate this degree for the composites, the Lotgering factor, *LF*, was calculated by analysis of XRD patterns. The room-temperature values of *LF*, electrical resistivity (ρ), Seebeck coefficient (S), total thermal conductivity (k) and thermoelectric figure-of-merit (ZT) are collected in Table 1.

LF is x-dependent and reaches maximum for x = 1.25 at.%. The thermoelectric properties are given for the perpendicular and parallel measuring orientations. The better thermoelectric properties are observed for the perpendicular measuring direction. S is very weakly x-dependent, whereas ρ and k changed with increasing x in complicated manner. However, combination of ρ, S and k for the composites allows remarkably enhancing their thermoelectric figure-of-merit, $ZT = TS^2/\rho k$ (T is the absolute temperature). Highest $ZT \approx 0.56$ found for the composite with x = 0.50 at.% for the perpendicular measuring direction. To find correct physical mechanisms, responsible for changes in the thermoelectric properties, experimental work is in progress.

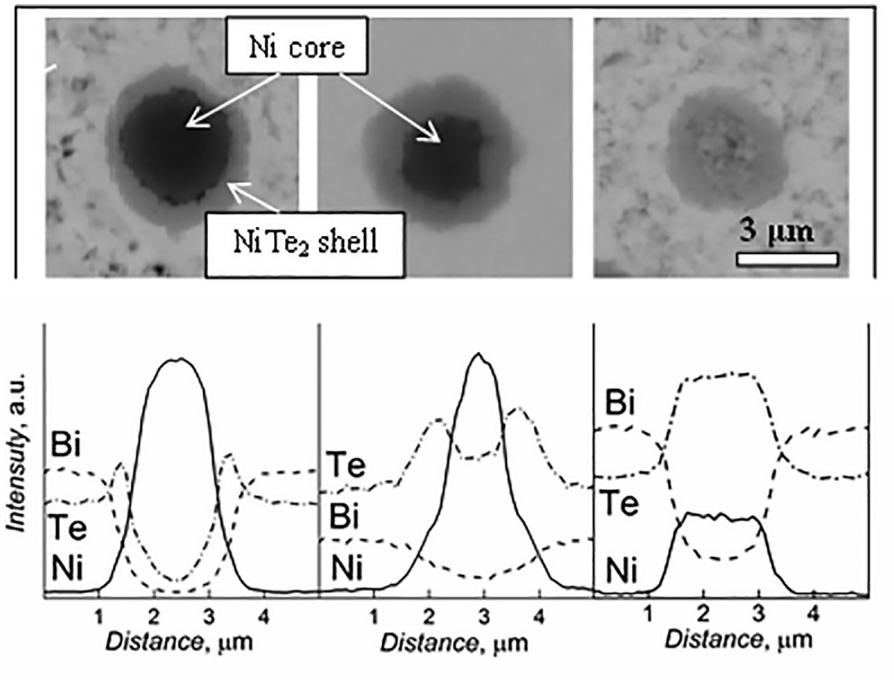

Fig. 3. The filler Ni@$NiTe_2$ inclusions (upper panel), and EDS-line scan profiles of Te, Bi and Ni distributions taken along lines crossing the inclusion (bottom panel); left part – the inclusion with $d > l$, medium part – the inclusion with $d \approx l$ and right part - the inclusion with $l > d$.

Table 1
The Lotgering factor and thermoelectric properties of the composites.

x	*LF*	Measuring direction	ρ [μΩ·m]	S [μV·K^{-1}]	k [W·m^{-1}·K^{-1}]	*ZT*
0.00	0.02	Perpendicular	23.01	−142.3	1.42	0.18
		Parallel	30.12	−142.4	1.37	0.15
0.50	0.15	Perpendicular	6.08	−134.2	1.57	0.56
		Parallel	26.22	−147.3	0.86	0.28
0.85	0.17	Perpendicular	8.93	−141.6	1.58	0.47
		Parallel	30.54	−146.4	0.79	0.26
1.25	0.18	Perpendicular	6.48	−124.8	1.46	0.45
		Parallel	18.63	−144.4	0.94	0.35
1.50	0.12	Perpendicular	8.42	−135.7	1.53	0.42
		Parallel	23.82	−144.4	0.79	0.32

4. Conclusion

Thus, the locally-gradient Ni@$NiTe_2$ domains are really formed inside the thermoelectric Bi_2Te_3 matrix during SPS-process. The thermoelectric figure-of-merit of the composites with the domains is remarkably enhanced as compared to that of the matrix itself.

CRediT authorship contribution statement

Maxim Yaprintsev: Conceptualization. **Alexei Vasil'ev:** Investigation. **Oleg Ivanov:** Conceptualization, Writing - review & editing. **Marina Zhezhu:** Investigation. **Ekaterina Yaprintseva:** Investigation. **Vseslav Novikov:** Investigation.

Declaration of Competing Interest

The authors declare that they have no known competing financial interests or personal relationships that could have appeared to influence the work reported in this paper.

Acknowledgements

This work was supported by Ministry of Science and Higher Education of the Russian Federation (grant number No 0625-2020-0015).

References

[1] T.J. Reinhart, Overview of composite materials, in: S.T. Peters (Ed.), Handbook of Composites, Springer, Boston, MA, 1998, pp. 21–33.
[2] H.J. Goldsmid, Materials 7 (2014) 2577–2592.
[3] B.D. Cullity, C.D. Graham, Introduction to Magnetic Materials, IEEE Press, Piscataway, 2009.
[4] O. Ivanov, M. Yaprintsev, A. Vasil'ev, J. Sol. St. Chem. 290 (121559) (2020) 1–9.
[5] N. Zhang, T. Khan, H. Guo, et al., Adv. Mater. Sci. Eng. (2019) 1–18.
[6] W. Liu, X. Yan, G. Chen, Z. Ren, Nano Energy 1 (2012) 42–56.
[7] W. Zhao, Z. Liu, P. Wie, et al., Nature Nanotechol. 12 (2017) 55–60.